Journal of Applied Geophysics 132 (2016) 1–16

Contents lists available at ScienceDirect

Journal of Applied Geophysics

journal homepage: www.elsevier.com/locate/jappgeo

Understanding hydrothermal circulation patterns at a low-enthalpy thermal spring using audio-magnetotelluric data: A case study from Ireland

Sarah Blake [a,b,*], Tiernan Henry [b], Mark R. Muller [a,1], Alan G. Jones [a,2], John Paul Moore [c], John Murray [b], Joan Campanyà [a], Jan Vozar [a], John Walsh [c], Volker Rath [a]

[a] Dublin Institute for Advanced Studies, Ireland
[b] Earth and Ocean Sciences, School of Natural Sciences, National University of Ireland, Galway, Ireland
[c] Fault Analysis Group, University College Dublin, Ireland

ARTICLE INFO

Article history:
Received 27 December 2015
Received in revised form 27 May 2016
Accepted 22 June 2016
Available online 27 June 2016

Keywords:
Audio-magnetotellurics
Three-dimensional inversion
Low-enthalpy geothermal exploration
Thermal springs
Ireland

ABSTRACT

Kilbrook spring is a thermal spring in east-central Ireland. The temperatures in the spring are the highest recorded for any thermal spring in Ireland (maximum of 25 °C). The temperature is elevated with respect to average Irish groundwater temperatures (9.5–10.5 °C), and represents a geothermal energy potential, which is currently under evaluation. A multi-disciplinary investigation based upon an audio-magnetotelluric (AMT) survey, and hydrochemical analysis including time-lapse temperature and chemistry measurements, has been undertaken with the aims of investigating the provenance of the thermal groundwater and characterising the geological structures facilitating groundwater circulation in the bedrock.

The three-dimensional (3-D) electrical resistivity model of the subsurface at Kilbrook spring was obtained by the inversion of AMT impedances and vertical magnetic transfer functions. The model is interpreted alongside high resolution temperature and electrical conductivity measurements, and a previous hydrochemical analysis.

The hydrochemical analysis and time-lapse measurements suggest that the thermal waters have a relatively stable temperature and major ion hydrochemistry, and flow within the limestones of the Carboniferous Dublin Basin at all times. The 3-D resistivity model of the subsurface reveals a prominent NNW aligned structure within a highly resistive limestone lithology that is interpreted as a dissolutionally enhanced strike-slip fault, of Cenozoic age. The karstification of this structure, which extends to depths of at least 500 m directly beneath the spring, has provided conduits that facilitate the operation of a relatively deep hydrothermal circulation pattern (likely estimated depths between 560 and 1000 m) within the limestone succession of the Dublin Basin. The results of this study support the hypothesis that the winter thermal maximum and simultaneous increased discharge at Kilbrook spring is the result of rapid infiltration, heating and re-circulation of meteoric waters within this structurally controlled hydrothermal circulation system.

This paper illustrates how AMT may be useful in a multi-disciplinary investigation of an intermediate-depth (100–1000 m), low-enthalpy, geothermal target, and shows how the different strands of inquiry from a multi-disciplinary investigation may be woven together to gain a deeper understanding of a complex hydrothermal system.

1. Introduction

Deep hydrothermal systems are well-established geothermal exploration targets. The potential of these systems is now being investigated in Ireland as part of the IRETHERM project (funded by Science Foundation Ireland). A multi-disciplinary approach has been adopted, integrating geophysical surveys and hydrochemical analysis with the aims of (1) identifying the source aquifer(s) for the thermal groundwater, (2) characterising the circulatory systems, and (3) assessing the potential for the existence of deeper, higher temperature, circulation patterns for future geothermal exploitation. A number of thermal springs have been identified that are currently being investigated. This paper presents a case study of one of these, Kilbrook spring, which has the highest recorded temperatures of any thermal spring in Ireland

* Corresponding author at: Dublin Institute for Advanced Studies, 5 Merrion Square, Dublin 2, Ireland.
E-mail address: sblake@cp.dias.ie (S. Blake).
[1] Now: Independent geophysical consultant, Cambridge, U.K.
[2] Now at: Complete MT Solutions, Ottawa, Canada.

http://dx.doi.org/10.1016/j.jappgeo.2016.06.007
0926-9851/

(maximum of 25.0 °C recorded during this study). This study shows how the use of geophysics as part of a multi-disciplinary investigation can result in a better understanding of the operation of a low-enthalpy hydrothermal system.

In Ireland, average groundwater temperatures typically range from 9.5 to 10.5 °C (Aldwell and Burdon, 1980) and thermal springs are considered to be those natural groundwater springs where the mean annual temperature is appreciably warmer than average groundwater temperatures (Aldwell and Burdon, 1980; Goodman et al., 2004). The spring is located in east-central Ireland (Fig. 1) and was first discovered in the late 19th century when the nearby Royal Canal was constructed (Burdon, 1983). The spring discharges from a glaciofluvial sand and gravel deposit in a disused quarry, which is located between the urban centres of Enfield, Co. Meath, and Kilcock, Co. Kildare. The temperature

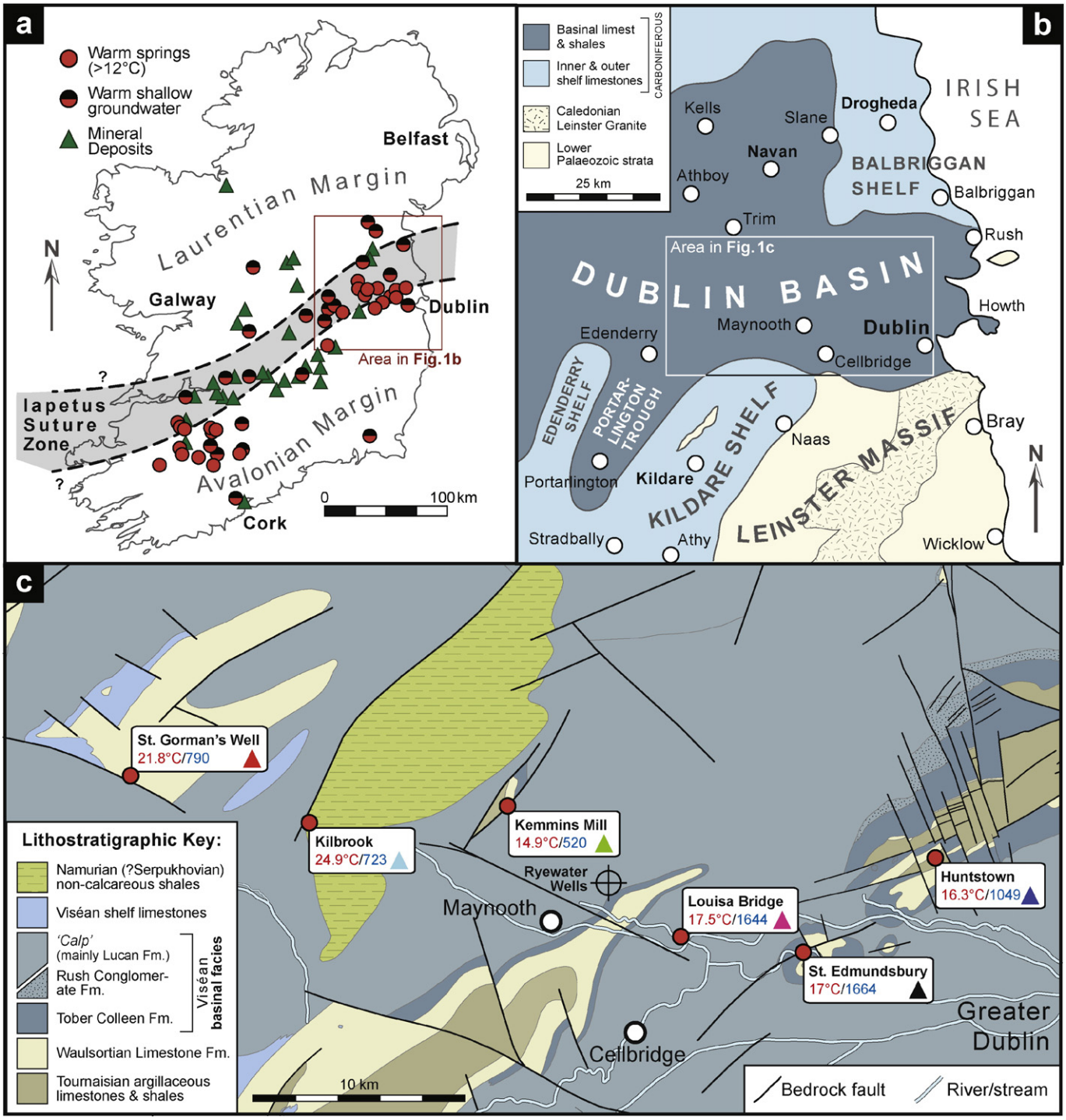

Fig. 1. Geological setting of Irish thermal groundwaters, sourced from Blake et al. (2016): (a) Irish thermal spring and thermal shallow groundwater locations (after Goodman et al., 2004), with significant mineral deposits and the approximate trace of the Iapetus Suture Zone (after Wilkinson, 2010); (b) palaeogeographic map of the Dublin Basin during the Viséan Stage (modified from Sevastopulo and Wyse Jackson (2009)); and (c) geological map of the study area (from www.gsi.ie) showing warm springs included in the hydrochemical sampling programme. Maximum temperatures (red) and mean electrical conductivities in μS/cm (blue) are given for each thermal spring. Coloured triangles in each of the thermal spring labels refer to colour coding used for these locations in subsequent figures. Further information on the springs can be found in the supplementary material.

profile of Kilbrook spring is consistently high and varies little throughout the year, with a mean temperature of 24.0 °C. The maximum discharge occurs in winter (857 m^3/d measured in January 1982; see Burdon, 1983) with a mean discharge of 472 m^3/d. This combination of relatively high discharge and high temperature is an encouraging indicator of the geothermal energy potential of the spring.

The audio-magnetotelluric (AMT) method is an electromagnetic geophysical technique that is widely used for exploring geothermal resources (e.g., Arango et al., 2009; Barcelona et al., 2013; Piña-Varas et al., 2014; Zhang et al., 2015) and hydrogeological targets (e.g., Falgàs et al., 2011; Kalscheuer et al., 2015) due to its ability to detect low-resistivity, water-bearing rocks in the subsurface. AMT is a passive electromagnetic technique that uses high-frequency, natural source fields generated by worldwide lightning activity. Compared to magnetotellurics (MT), it is useful for characterising the shallow subsurface. The depth of penetration for AMT can be up to several hundred metres and even greater than a kilometre, depending on the resistivity of the bedrock. When used as part of a multi-disciplinary approach (incorporating geological, hydrogeological, and other geophysical data), AMT is an efficient and relatively inexpensive method for improving the characterisation of a geothermal resource (compared to other methods of geophysical exploration, or to drilling).

In this paper we present a new model from an AMT survey at Kilbrook spring. The twin overarching goals of the AMT survey were (1) to identify any (electrically conductive) fluid conduit systems associated with the thermal spring and (2) to assess the nature and extent of the hydrothermal circulation pattern. The results are discussed alongside detailed time-lapse measurements of temperature and electrical conductivity, and hydrochemical data collected seasonally at the spring.

2. Kilbrook spring in context

2.1. Geology and hydrogeology

Irish thermal springs occur in areas of Carboniferous limestone bedrock (the unweathered rock beneath unconsolidated material) along a wide band that traverses the centre of Ireland from NE to SW. The locations of the springs are broadly coincident with the putative trend of the Lower Palaeozoic Iapetus Suture Zone (ISZ) (Fig. 1 a)). The ISZ was produced by the final closure of the Iapetus Ocean in late Silurian times, during the later stages of the Caledonian Orogenic cycle (e.g., Chew and Strachan, 2014). Following collision, terrestrial sediments were deposited during the Devonian period (e.g., Graham, 2009), before a shift to predominantly carbonate deposition as a result of a regional marine transgression during earliest Carboniferous (Tournaisian) times (MacDermot and Sevastopulo, 1972). During the Tournaisian and Viséan, several intra-cratonic basins developed across Ireland as a result of tectonism and subsidence (e.g., de Morton et al., 2015; Somerville, 2008; Strogen et al., 1996), principally controlled by movement on NE–SW oriented structures, whose orientation was inherited from underlying Caledonian trending features (Worthington and Walsh, 2011). Extensive carbonate production continued in Ireland for much of the Mississippian, before a switch to terrigenous mud and sand deposition in the Serpukhovian and Bashkirian (formerly regionally termed the Namurian in northwest Europe: see Sevastopulo, 2009; Barham et al., 2015).

Kilbrook spring is situated in the Carboniferous Dublin Basin (Fig. 1 b)), which contains circa 2000 m of sedimentary infill and saw the widespread development of carbonate buildups ('reefs') during late Tournaisian to early Viséan times (Somerville et al., 1992). This particular facies, commonly termed the Waulsortian Limestone Formation, is characterised by very fine-grained, pure carbonates containing sparry masses. Bedding within the carbonate buildups is often indistinct: these buildups commonly formed aggregates, and intervening, off-mound facies are typically represented by thin, nodular, chert-rich shales (Lees and Miller, 1995). The relative purity of this carbonate facies results in it being prone to chemical dissolution and the development of karst features, which is an important consideration for modern groundwater circulation. Active tectonism during the Viséan age led to the development of shallow shelf platforms and contrasting deeper regions in the Dublin Basin. The deeper basinal facies is characterised by thinly inter-bedded, cherty limestones and shales (mapped regionally as the Lucan Formation, or "Calp"; see Marchant and Sevastopulo, 1980). Kilbrook spring occurs near the lithostratigraphic contact between the Lucan Formation and younger Namurian non-carbonate bedrock (Figs. 1 c) and 2). The spring discharges from a surficial glaciofluvial deposit consisting of coarse sands and gravels. This deposit covers an area of 0.32 km^2, has an oblate shape oriented NW to SE, and may infill a depression in the surface of the underlying bedrock. Bedrock exposure in the area is generally poor, and there are limited borehole records available. Two boreholes were completed in 1983 by the Geological Survey of Ireland (GSI) (Fig. 2):

- Extremely weathered bedrock was encountered at a depth of 23 m in one borehole adjacent to the spring pond; this material resembled a fault breccia (Burdon, 1983), indicating the proximity of the spring to a significant geological structure.
- A second borehole was completed at a depth of 24 m without encountering bedrock (Murphy and Brück, 1989).

Kilbrook spring is situated 35 km west of Dublin, in a relatively flat and low-lying landscape in the Eastern River Basin District. The elevation in the survey area (Fig. 2) ranges from approximately 80 to 100 m above ordnance datum. The 30-year (1981–2010) average annual rainfall in the area is 868 mm/yr (Walsh, 2012); during the sampling period (for the hydrochemical sampling and time-lapse measurements) the annual rainfall was 863 mm in 2013 and 922 mm in 2014 (data from Met Éireann, www.met.ie). Evaporative losses for the region are estimated at 450 mm/yr (Met Éireann). The main use of land is agricultural, and the spring itself is situated in a disused gravel pit. The Lucan Formation is classified by the GSI as "locally important, moderately

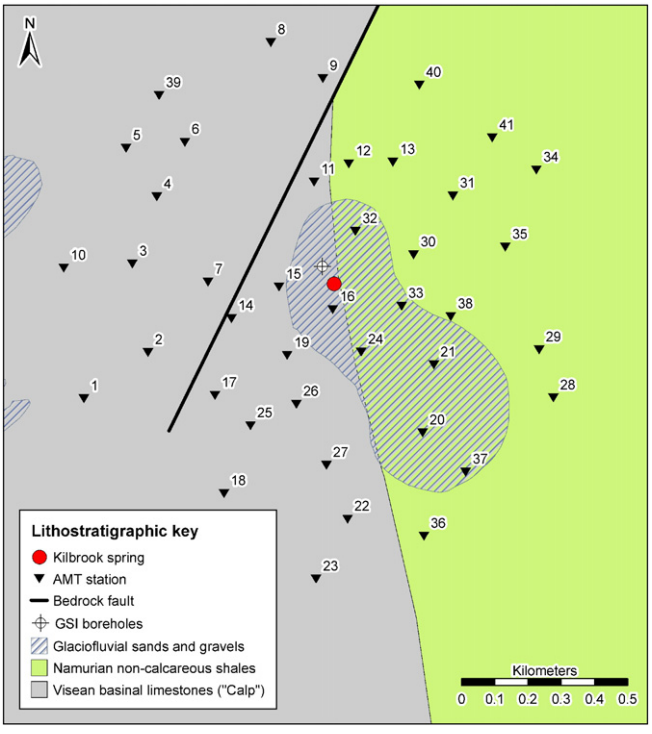

Fig. 2. AMT station locations and local geology (from www.gsi.ie) at Kilbrook spring. The spring is located at 53°25′24.23″N 6°46′31.63″W.

productive" aquifer, and the Namurian shales and sandstones are classified as "poor aquifer, generally unproductive". Most recharge to aquifers in Ireland occurs in the period between October and April, and typical estimated recharge rates for this area are between 101 and 200 mm/yr (Hunter Williams et al., 2011).

The pond at Kilbrook spring is largest during winter, in the high recharge period between October and April, when its surface area is approx. 100 m^2. In the summer, the discharge decreases and the area of the pond is reduced. Water flows northward from this pond to a larger pool, then discharges to a land drain 150 m north of the spring. The discharge of the spring was monitored on a monthly basis between 1981 and 1983 (Burdon, 1983), and from these data the discharge is estimated to be approximately 860 m^3/d during the winter, with a yearly average of 470 m^3/d. No detailed hydrodynamic data were available for this study area.

The water from Kilbrook spring has a calcium-bicarbonate hydrochemical signature, typical of many recently infiltrated, cold, Irish groundwaters circulating in limestones, and also typical of the majority of the Irish thermal springs. Irish thermal springs tend to have a predominantly meteoric hydrochemical signature (Burdon, 1983; Mooney et al., 2010), implying that they are mainly composed of waters that are recharged from relatively recent rainfall events. Burdon (1983) showed that Kilbrook spring contained lower tritium levels and higher ^{4}He levels than cold groundwater. These low tritium levels, along with the elevated temperatures, are suggestive of longer residence times and a deeper circulation pattern for the thermal groundwater. Water samples recovered from Kilbrook spring are likely to be a blend of groundwaters from different sources and different recharge areas. The thermal water could be composed of a mixture of a deeper-circulating, older groundwater, and more recent, meteoric recharge water from a shallow groundwater system.

2.2. Structural geology

The Carboniferous limestones in Ireland that host the thermal springs generally tend to exhibit poor primary porosity. Secondary porosity and permeability are greatly improved by both fracture and karst development, providing discrete pathways for groundwater flow; it is therefore important to consider structural controls on fluid flow within these limestones. In carbonates, the development of deep dissolutional features (at depths of at least 500 m) is likely to be controlled and facilitated by prominent fault structures (Kaufmann et al., 2014). Irish thermal springs are frequently associated with deep-seated, high-angle faults, which facilitate the movement of warm waters towards the surface (Mooney et al., 2010), and they appear to be associated with the dominant NE–SW structural lineaments apparent in Ireland's bedrock (Fig. 1 a)). These deep-seated, pervasive faults, although no longer tectonically active, may still provide fluid pathways enhanced by dissolutional processes in discrete zones (through karstification), allowing water to flow from deeper units up to the surface, and are probably very important in controlling regional groundwater flow (Henry, 2014).

The development of secondary porosity in the Waulsortian Limestone Formation is likely to contribute to the development of thermal springs in the Dublin Basin, as four out of six thermal springs studied in detail during the IRETHERM project issue from, or have a close spatial association with, mapped surface outcrop of Waulsortian strata, as can be seen in Fig. 1 c) (for more details, see supplementary material, Table A). While Kilbrook spring issues from supra-Waulsortian strata, the Waulsortian Limestone Formation may exist beneath these strata. The centres of Waulsortian buildups are typically massive (see Lees and Miller, 1995), so any karstic dissolution will tend to exploit areas of fissured and fractured rock. By comparison, the chert-rich, off-mound facies are much less soluble, and may thus act to constrain or focus groundwater flow. Flow within discrete Waulsortian mounds can become concentrated along vertical or sub-vertical pathways with relatively little lateral dissipation of flow (Moore et al., 2015).

Dissolutional features in the Waulsortian limestones in the Dublin Basin near St. Gorman's Well (Fig. 1 c)) have been reported at depths of 250–300 m (borehole reports from www.mineralsireland.ie) and may possibly exist at 510 m in one reported instance (Murphy and Brück, 1989). These features play an important role in the operation of deep groundwater circulation patterns and facilitate the movement of the thermal spring waters to the surface.

A significant (28 km) NE–SW oriented normal fault is present close to Kilbrook spring on the geological map (Figs. 1 and 2), juxtaposing downthrown Namurian sediments to the east and upthrown Lucan Formation limestones to the west. The trend on this fault is Caledonian and it is likely that it is deep-seated, and of Carboniferous age. These Carboniferous normal faults were subsequently reactivated as thrust faults during later compressional tectonic events (e.g., Hitzman, 1999), leading them to act as impermeable barriers to groundwater flow; this occurs mainly because they are enriched with incorporated host-rock clays and shales by a combination of fault rock attenuation and smearing, and by dissolution-related restite formation (Moore and Walsh, 2013). In certain locations, particularly where they are intersected by N–S oriented, Cenozoic, strike-slip faults, they can become karstified and have their permeability greatly increased (Moore and Walsh, 2013). A local example of such an intersection of structures can be seen at Rathcore Quarry, six kilometres west of Kilbrook spring. Here, the intersection of a Carboniferous normal fault and a N–S oriented Cenozoic strike-slip fault has resulted in the development of a large karstic depression (20 m wide), which has been subsequently filled with unconsolidated materials.

3. AMT survey

The AMT method determines the distribution of the electrical properties of the subsurface and the results can be expressed in terms of electrical conductivity (S/m) or electrical resistivity (Ωm). Conductivity and resistivity are inversely related so that a body with high resistivity will have a low conductivity, and vice versa. Here, the results of the AMT survey are expressed in terms of resistivity, with equivalent conductivity values supplied for context.

3.1. AMT method

The MT method is a geophysical technique that determines the distribution of electrical resistivity in the subsurface by relating simultaneous measurements of the naturally occurring fluctuations of the electric and magnetic fields at the Earth's surface. Recent comprehensive reviews of the MT method are provided by Simpson and Bahr (2005), and Chave and Jones (2012). Natural electromagnetic fields that are utilised as source fields in MT studies range in frequency from approx. 10^{-5} to 10^5 Hz. Audio-magnetotelluric (AMT) studies utilise higher frequency (>8 Hz) electromagnetic waves that are generated by electric lightning discharge during lightning storms and propagate around the globe in the Earth-ionosphere waveguide. Commonly, a frequency interval with poor signal-to-noise ratio is found between 1000 Hz and 5000 Hz, which is called the AMT "dead-band". García and Jones (2005) demonstrated that night-time signals are usually strong enough to provide good estimates of the transfer functions of AMT dead-band frequencies, with maximum signal strength occurring around local midnight. For this reason, the AMT soundings for this survey were carried out overnight to maximise the data quality.

3.2. AMT dataset

The AMT survey was designed to target any karstified conduits occurring beneath the thermal spring at Kilbrook. Forty-one AMT measurement locations (stations) were laid out in an approximate grid pattern, centred on the spring itself, with approx. 200 m between sites

(Fig. 2). The grid covered a total area of 2.7 km^2. This layout was chosen to investigate depths in excess of 100 m beneath the spring (with a separation of 200 m between stations at the surface, the volumes of measurement beneath each of the stations first overlap at a depth of around 100 m, thus providing a more reliable estimation of the properties of the subsurface at depths greater than 100 m.) The survey was carried out in July 2012. Overnight AMT measurements were made using Phoenix MTU-5 systems with an electrode array and horizontal magnetic coil configuration oriented to geomagnetic north–south-east–west, combined with a vertical magnetic recording at each station. Data were acquired in the frequency range between 1 Hz and 10,000 Hz. As the data quality in populated areas is often affected by man-made ("cultural") electrical noise, one system was deployed as a remote magnetic reference station in a culturally quiet location approximately 4.6 km NE of the spring. This extra station allowed for remote reference processing (Gamble et al., 1979). The AMT time series were processed using Phoenix SSMT2000 software, which employs a robust variant of a remote reference processing algorithm based on Jones and Jödicke (1984), and Jones et al. (1989). Aside from the aforementioned AMT dead-band, the data quality was generally good between 10 Hz and 10,000 Hz. The impedance tensors (**Z**) and the vertical magnetic transfer functions (**T**) were estimated for each frequency for each station. Each curve was manually edited to remove excessively noisy data in the AMT dead-band.

3.3. Dimensionality analysis

The dimensionality of the data was analysed by investigating the **Z** and **T** responses independently of each other. For the **Z** responses, the dimensionality analysis was performed by examining the phase tensors (Caldwell et al., 2004), which have the advantage of being unaffected by galvanic distortion of the electric fields. Fig. 3 shows the calculated

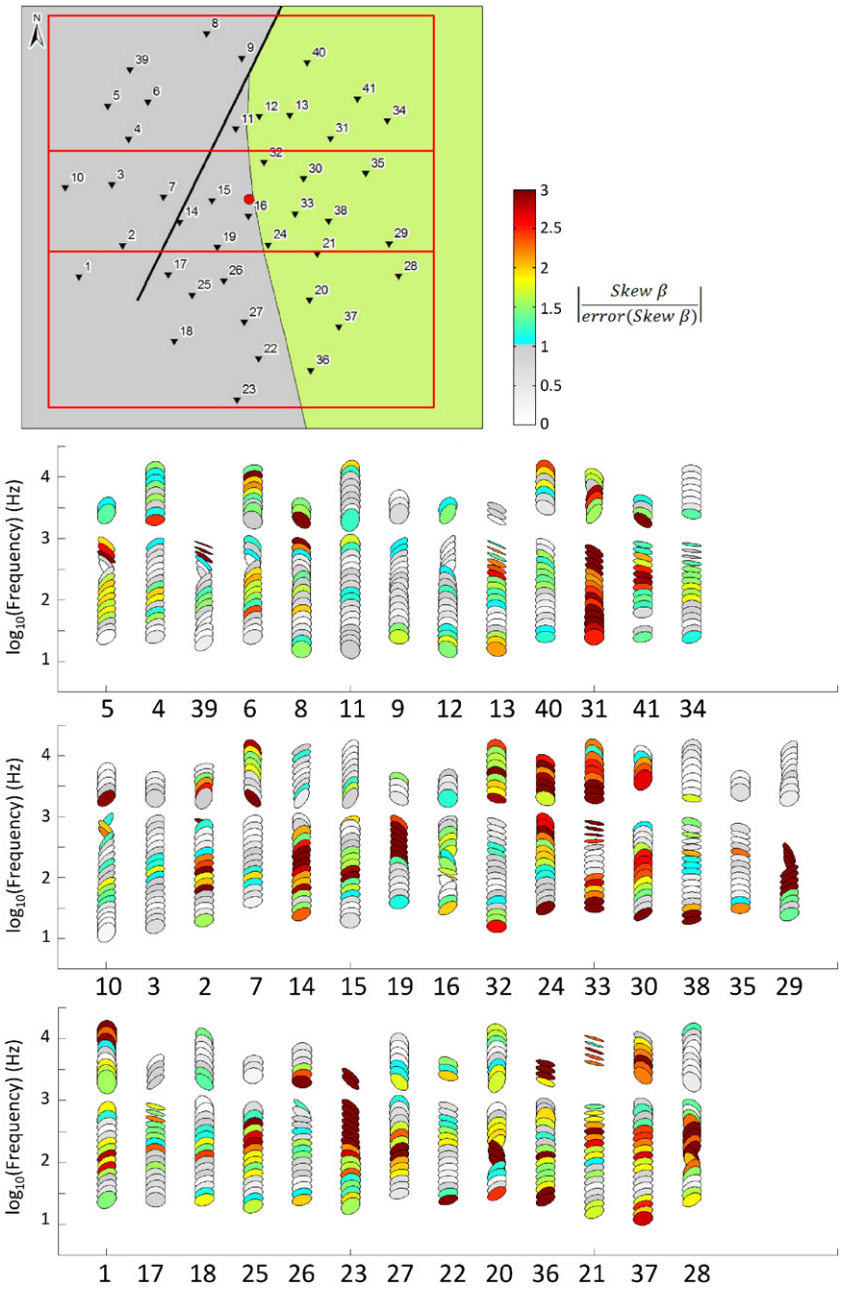

Fig. 3. Phase tensor dimensionality analysis using **Z** responses. White-grey colours indicate frequencies affected by the presence of 1-D or 2-D structures. Other colours represent frequencies affected by 3-D structures. The stations are arranged from W to E in three panels to correspond with the boxes outlined in the map of the survey area (Fig. 2).

phase tensor for each frequency for each station, depicted as an ellipse. For a 1-D scenario the phase tensor will be represented by a circle, and for a 2-D case the phase tensor will be represented by a symmetrical ellipse, with the orientation of the major axis aligned either parallel or perpendicular to the regional geoelectrical strike direction. For 3-D cases the phase tensor will be non-symmetrical, necessitating the use of an additional angle, β, to characterise the tensor. In Fig. 3, the ellipses representing 3-D conditions are coloured depending upon the magnitude of β normalised by the corresponding error, following the approach of Campanyà et al. (in review). All stations in Fig. 3 show coloured ellipses for some frequencies, indicating 3-D conditions for the survey area. For the **T** responses, induction arrows (Schmucker, 1970) following the Parkinson criteria (i.e., the real arrows tend to point towards current concentrations in conductive anomalies (Jones, 1986)) were used. Fig. 4 shows the induction arrows for each station and each frequency (station 33 has no induction arrows because the **T** data quality was poor for this station). For a 1-D scenario the length of the induction arrows will be less than the threshold length of the assumed errors as there is no induced vertical magnetic field. For a 2-D scenario the induction arrows will point in the same or exactly opposite directions for all periods and stations. In a 3-D scenario, real and imaginary induction arrows will point in different (oblique) directions at any one frequency for any station (as can be seen in Fig. 4). The results from Figs. 3 and 4 indicate the existence of a 3-D scenario beneath the survey area.

3.4. 3-D inversion

Based upon the results of the dimensionality analysis, 3-D inversion was adopted as the most appropriate course of action. AMT data from 28 frequencies (excluding frequencies in the dead-band, particularly between 800 Hz and 2000 Hz) were prepared for the inversion; these

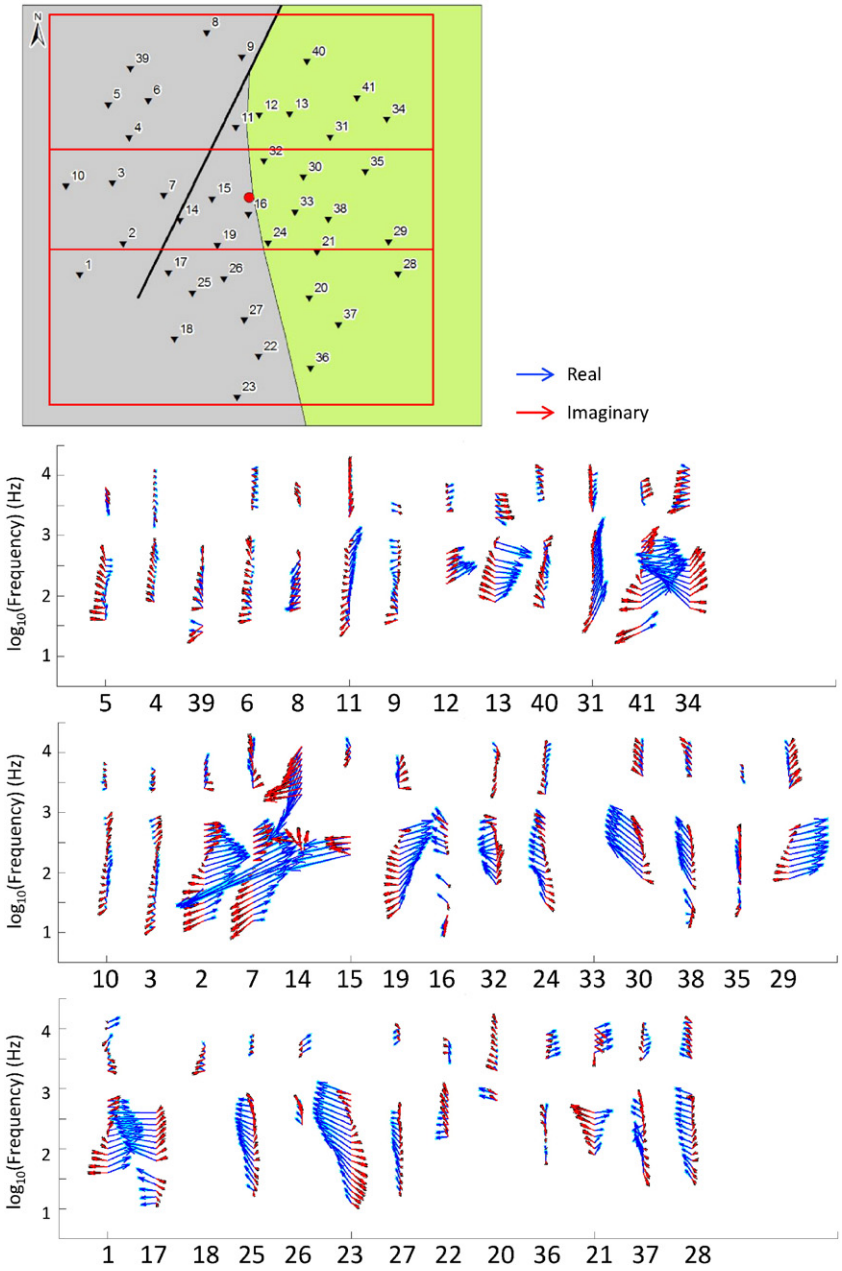

Fig. 4. Induction arrow dimensionality analysis using **T** responses, following the Parkinson criteria. The stations are arranged from W to E in three panels to correspond with the boxes outlined in the map of the survey area (Fig. 2).

data were subsequently re-edited on a station-by-station basis to remove particularly noisy frequencies. The data were inverted using the ModEM 3-D inversion code (Egbert and Kelbert, 2012; Kelbert et al., 2014). The vertical magnetic transfer functions (**T**) were inverted alongside the four components of the impedance tensors (**Z**) to improve the resolution of the subsurface resistivity values (e.g., Siripunvaraporn and Egbert, 2009; Campanyà et al., in review). The mesh for the resistivity model consisted of 90 × 90 × 90 cells, with square cells with sides 50 m long in the horizontal plane of the central region of interest. This central region was a square with sides 3 km long. Padding cells were added in the *x* and *y* directions with an incremental factor of 1.3. In the *z* direction, 10 air layers were added above the resistivity model. The first (surface) layer of the model was 10 m thick; these layers were incrementally increased by a factor of 1.025 until a thickness of 60 m was achieved. The layers were then increased by a factor of 1.1. The final model dimensions were 8 km × 8 km × 5 km. Several preliminary models were assigned a homogeneous half space with varying resistivity values as their starting and prior models; the best results (i.e., with the least extreme values and resolving the most structure) were obtained with half-spaces of 300 and 500 Ωm (0.003 and 0.002 S/m). An average of four models (two starting models with homogeneous half-spaces of 300 Ωm and 500 Ωm, and the two resultant models from those inversions) was calculated and set as the prior model for the final inversion. The model mesh was not rotated, as advocated by Kiyan et al. (2014), as preliminary models showed the subsurface to have 3-D structure with no one predominant geoelectrical strike direction evident. An error floor of 5% was imposed for all components of **Z** (calculated from the modulus of the off-diagonal components $\mathbf{Z}_{xy}$ and $\mathbf{Z}_{yx}$), and an absolute error of 0.03 was used for **T**. Variation of the smoothing parameters was investigated for the model; values between 0.1 and 0.5 were tested, and an intermediate value of 0.3 (in all directions) for the smoothing parameter gave the minimum root mean square (RMS) misfit for the data.

No correction or compensation was applied to the data to account for galvanic distortion, which is a tractable problem in 2D cases, but far less important in 3D (see Jones, 2011). An examination of the apparent resistivity curves revealed no particular "problem areas" for galvanic distortion. As a 3-D modelling approach was used, with a fine parameterization in the uppermost part of the model, it was expected that the model would not be greatly affected by near-surface galvanic distortion effects at our target depths (e.g., Sasaki and Meju, 2006; Farquharson and Craven, 2009; Meqbel et al., 2014). Also, the inversion of **T** alongside **Z** should decrease the susceptibility of the model to the effects of galvanic distortion as **T** is not affected by galvanic distortion of the electric field, only of the magnetic field. The resulting models do not show obvious artefacts (i.e., site-correlated model structures), which commonly indicate the presence of static shifts.

3.5. Final model

The final resistivity model converged after 38 iterations with a RMS misfit of 2.05. Fig. 5 shows the residual misfit of the data to the model responses for each period and each station. In general, the fit to $\mathbf{Z}_{yx}$ is better than to $\mathbf{Z}_{xy}$, and the lower frequencies show a poorer fit. Upon examination of the model, and given that the space between stations is approx. 200 m, the model results are more reliable from approx. 100 m depth. Resolution of fine structure decreases with depth, and is best resolved between depths of 100 and 500 m. There is a conductive region in the model between depths of 1500 and 3000 m, with resistivity values that are lower than the initial model. Beneath this conductive horizon, the values are the same as the initial model. This conductive region signifies the absolute extent of the sensitivity of the data to variations in resitivity.

The model shows a large region of high resistivity in the centre of the survey area (Fig. 6). At shallower depths, the spring is located on the NW edge of this resistive body, with more conductive material to the NW. There are two highly resistive cores within this high resistivity region with apparent resistivity values in excess of 5000 Ωm (<0.0002 S/m). The spring is situated on the linear boundary between these two resistive cores. This linear boundary is evident from depths of around 100 m to 800 m, has a lower resistivity than the surrounding material, and is oriented NNW. This feature is vertical or sub-vertical when viewed in profile (Fig. 10 b)). There is a region of low-resistivity material of between 10 and 500 Ωm (0.1 to 0.002 S/m) in the NW portion of the survey area. The boundary between this region and the resistive region is irregular with an approximate NE–SW trend. There is a large low resistivity pocket directly to the north of the spring, and this can be seen to extend to a depth of approx. 200 m (Fig. 7, P1). There is also a region of less resistive material east of the spring, on the edge of and to the east of the survey area; as there are no stations directly above this feature, it is not possible to properly resolve it, and so it is not discussed further here.

4. Discussion

The results from time-lapse temperature measurements, hydrochemical analysis and the AMT survey are discussed here to develop an integrated conceptual model for the hydrothermal circulation pattern at Kilbrook thermal spring.

4.1. Time-lapse temperature measurements

Continuous temperature and electrical conductivity (EC) measurements were collected at Kilbrook spring between July 2013 and April 2015 (Fig. 8). The EC data are presented in μS/cm (1 μS/cm is equivalent to 0.0001 S/m). Further information regarding data collection is available in the supplementary material (or see Blake et al., in press). In general, the temperature readings proved to be reliable, but the EC readings appear to have been adversely affected by the influence of fouling by bacterial growths on the sensors. This is evident in Fig. 8, where the EC readings appear very unstable after any re-installation of the logger. From seasonal field measurements using a Hanna HI 98130 Combo metre (measurements indicated in Fig. 8 and Table 1), the EC of Kilbrook spring appears to be fairly stable (maximum of 652 μS/cm and a mean of 634 μS/cm).

The temperature profile for the first year (July 2013–June 2014; Fig. 8) shows remarkably stable temperatures that are lower at the end of the summer (between August and November), and slightly higher in winter (after December). This general profile of higher temperatures in winter is repeated in the second year (July 2014–April 2015). The summer period in the first year has slightly lower temperatures than in the subsequent year (approx. 23.5 °C compared to 24.5 °C for the second year). The period between August and November is characterised by a flashy signature with short-lived decreases in temperature to as little as 19.5 °C (October 2014). This flashy period has a longer duration in the first year. The month of November is marked by a gradual increase in temperature; higher temperatures are sustained throughout the winter and spring, with temperatures dipping again in August. The onset of the high-temperature, winter phase in November/December is gradual. A maximum temperature of 24.8 °C was recorded in the first year in June 2014, and a maximum of 25 °C was recorded in the second year at the end of January 2015.

Data from monthly discharge measurements made in 1982 (Burdon, 1983) show the discharge of the spring to be greatest in winter (particularly between December and April), and very low in summer (particularly between July and November). This suggests that the (hydrothermal) circulation pattern is controlled by annual recharge, and that the spring has a hydraulic connection to meteoric recharge processes occurring at the surface and in the shallow subsurface.

Despite an obvious connection to meteoric recharge processes, the largely steady temperature and EC (Table 1; Fig. 8) profile of Kilbrook spring supports the presence of, and influence from, a deeper aquifer

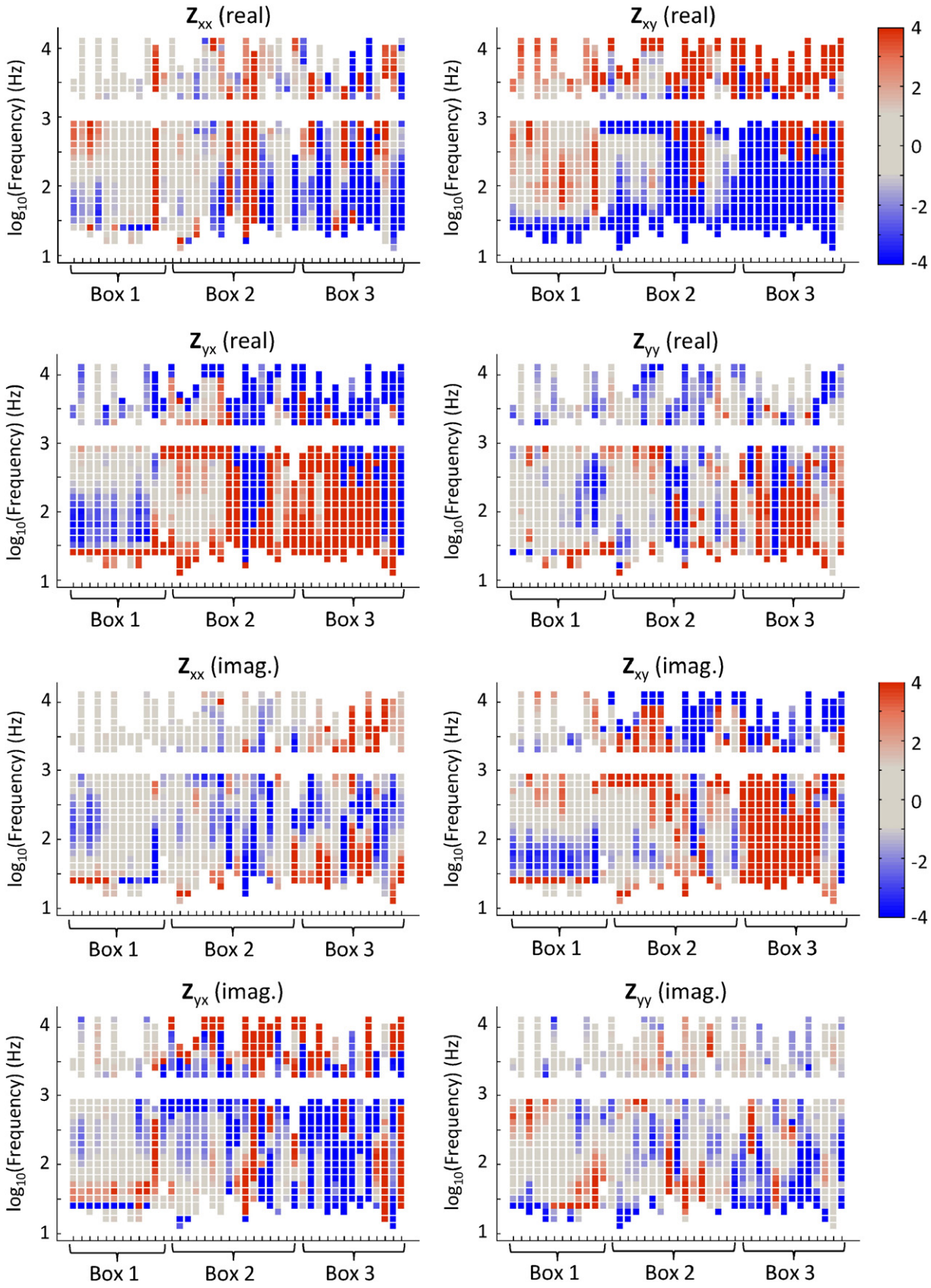

Fig. 5. Representation of the data fit to the model responses from the final 3-D inversion. Data from both components of T and all four components of ***Z*** are represented (real and imaginary parts). The stations are grouped to reflect the three boxes in the inset: the stations are arranged in order of their appearance from W to E. The coloured scale represents the difference between the data and the model response divided by the error for each frequency at each station.

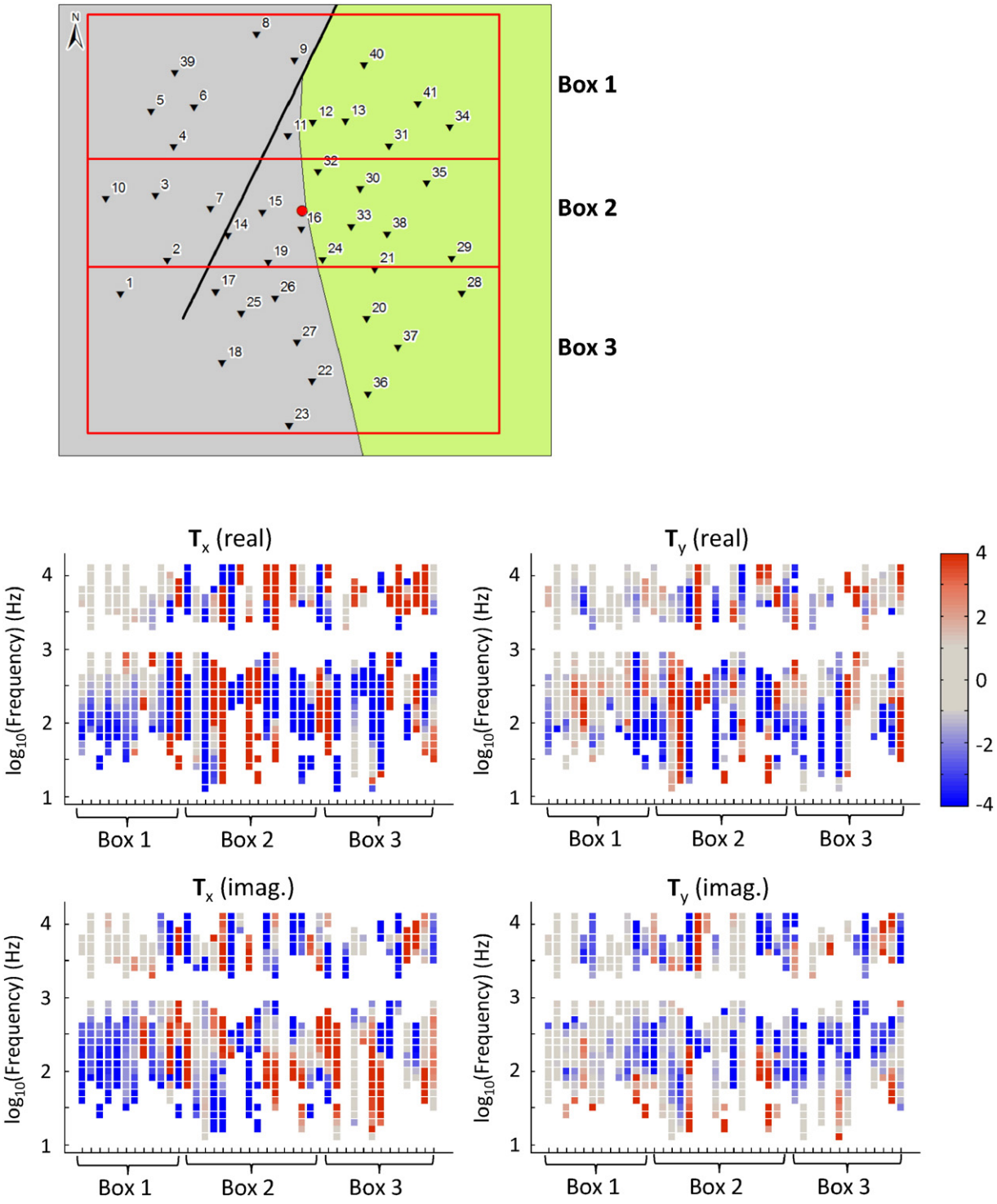

Fig. 5 (*continued*).

with a degree of insulation from near-surface recharge processes. The flashy profile towards the end of the summer (August to November), indicates the response of the spring to input of cooler recharge waters. However, this flashy signature does not continue beyond December into the winter period. It is possible that the increase in the regional water table due to the increase in recharge at the end of the summer period puts into operation a higher temperature, higher discharge circulation pattern at Kilbrook spring. This winter circulation pattern must be deep-seated, as it does not show any influence (delayed or otherwise) from rainfall events.

In both years the temperature profile exhibits diurnal and semi-diurnal fluctuations at certain times (see insets in Fig. 8), which are more pronounced in the summer when water levels are low. The diurnal fluctuations are partly influenced by the daily changes in temperature at the open pond surface. Semi-diurnal fluctuations in water level were first identified in 1982 (Burdon, 1983) and compared to gravity-tide-corrected data. The close correlation of the two signals confirmed the strong influence of the Earth's gravity tides upon the water levels in Kilbrook spring, with maximum variations occurring around the times of the new and the full moon (Burdon, 1983). The relative movements

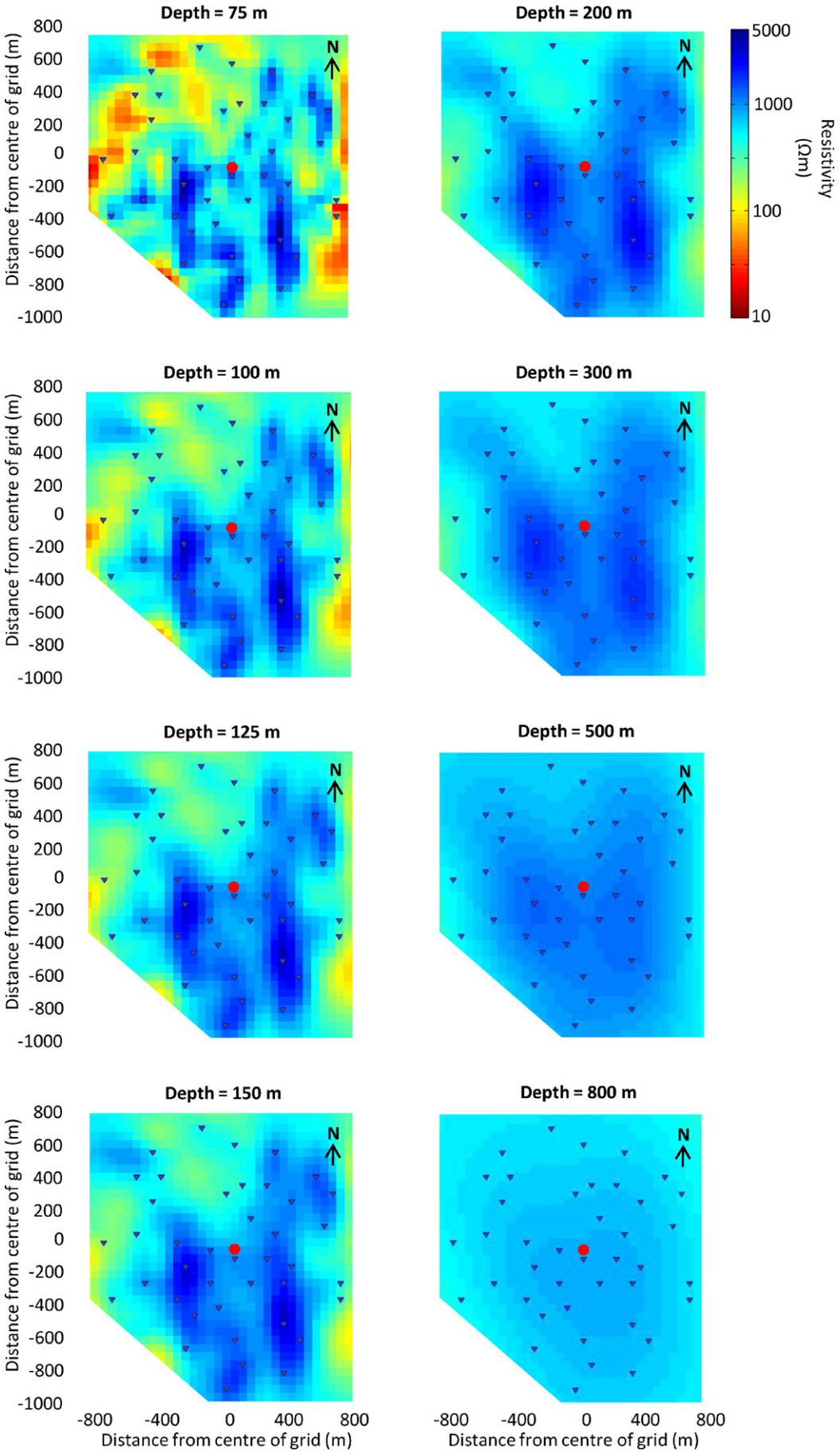

Fig. 6. Horizontal slices through the final 3-D resistivity model. The depth of each slice is indicated. The surface location of the spring is indicated by a red circle.

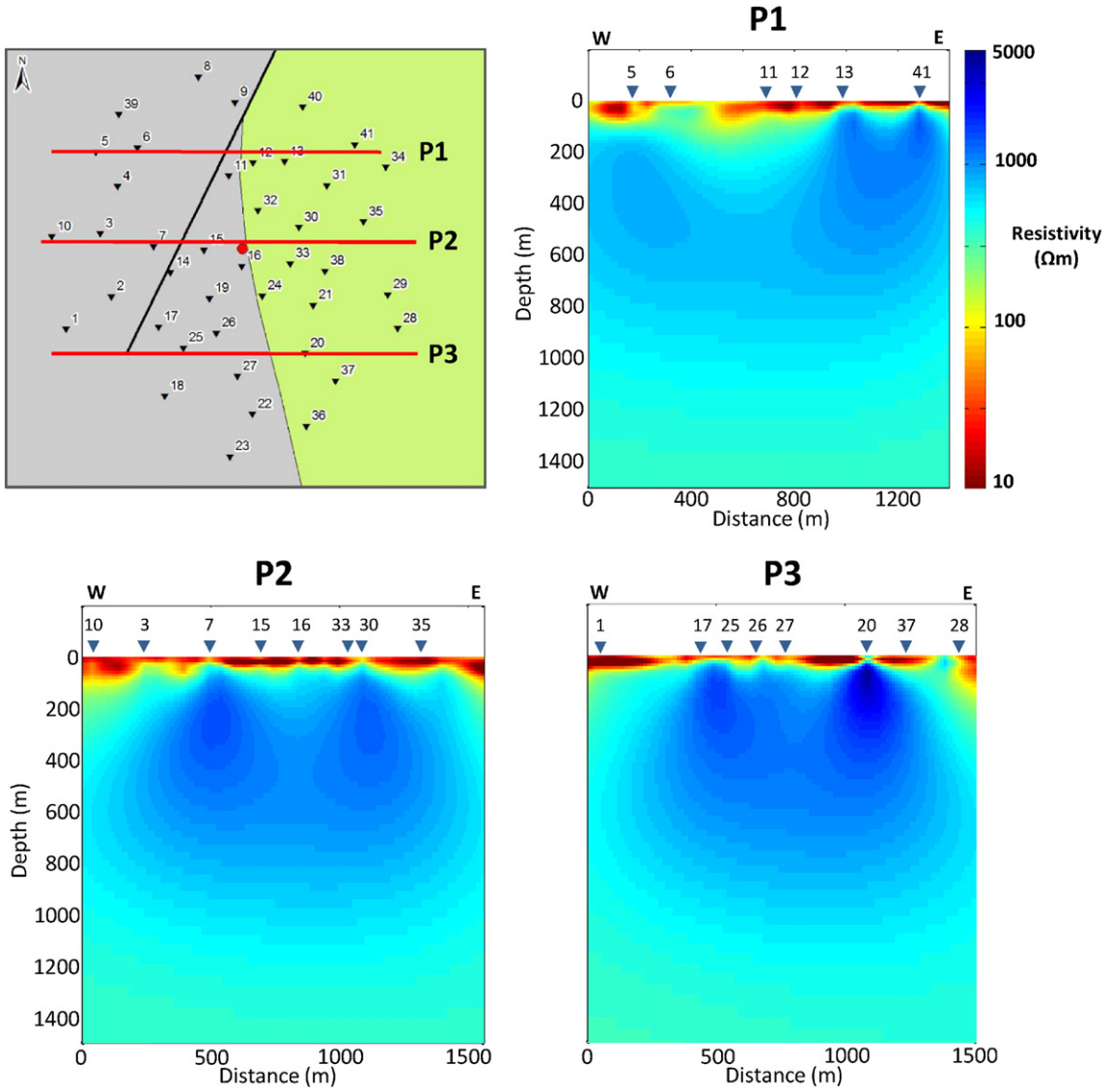

Fig. 7. Vertical profiles (P1, P2 and P3) through the final resistivity model. The profile locations are indicated in the plan view of the survey area. The locations of the AMT stations are indicated by inverted triangles.

of the Earth, Sun. and Moon cause a periodic distortion in the shape of the Earth that causes groundwater to be expelled from aquifers; this is often termed the tidal loading effect and is most measurable in aquifers in rigid, fractured rocks (e.g., Bodvarsson, 1970; Rojstaczer and Agnew, 1989; Maréchal et al., 2002; Lai et al., 2013). The presence of these semi-diurnal fluctuations in water level (Burdon, 1983) and temperature (this study) is evidence that both water level and temperature are controlled by tidal forces, and that the thermal groundwater is stored in a fractured, hard-rock aquifer. The semi-diurnal fluctuations still exist in the winter, but are less pronounced due to the increase in discharge.

4.2. Hydrochemical analysis

Several of the Irish thermal springs were sampled in July/August and October 2013, and in January, May and August 2014 (sampling times indicated on Fig. 8). This hydrochemical analysis is the subject of the paper by Blake et al. (in press), and details of the sample collection and analysis are provided in the supplementary material of this paper.

The major ion chemistry of Kilbrook spring during the sampling period (2013 to 2014) is comparable to Irish carbonate (Ca-HCO_3-type) groundwaters and reflects the findings of previous studies (Burdon, 1983). It is clear from Fig. 9 a) that the major ion hydrochemistry of the spring varies little throughout the year. Therefore, the majority of the groundwater supplying the spring must circulate in limestone bedrock. Two of the other springs have a notably saline hydrochemistry (St. Edmundsbury spring and Louisa Bridge Spa Well).

Previous work has suggested that Kilbrook spring (along with most Irish thermal springs) has a predominantly meteoric hydrochemistry; however, some indicators of a deeper circulation and a longer residence time exist (^{4}He and tritium analyses from Burdon (1983)). These indicators, along with slightly elevated levels of chloride, sodium and potassium, suggest that Kilbrook spring represents a mixture of shallow, recently recharged meteoric waters, and deeper, older, and more saline waters. From borehole records, it is estimated that the glaciofluvial deposit from which the spring emerges extends to a depth of at least 23 m. The higher Na concentrations at Kilbrook spring could be due to the buffering effect of this thickness of glaciofluvial sands and gravels, or it could be due to the interaction of the thermal waters with the Namurian non-calcareous shales, which are not present at any of the other thermal spring sites.

The relative amounts of sodium, chloride and bromide (the Na-Cl-Br system) were examined to assess the source of the excess chloride in the groundwater. The Cl/Br mass ratios were found to exceed 200 for Kilbrook and St. Edmundsbury springs, along with Louisa Bridge Spa

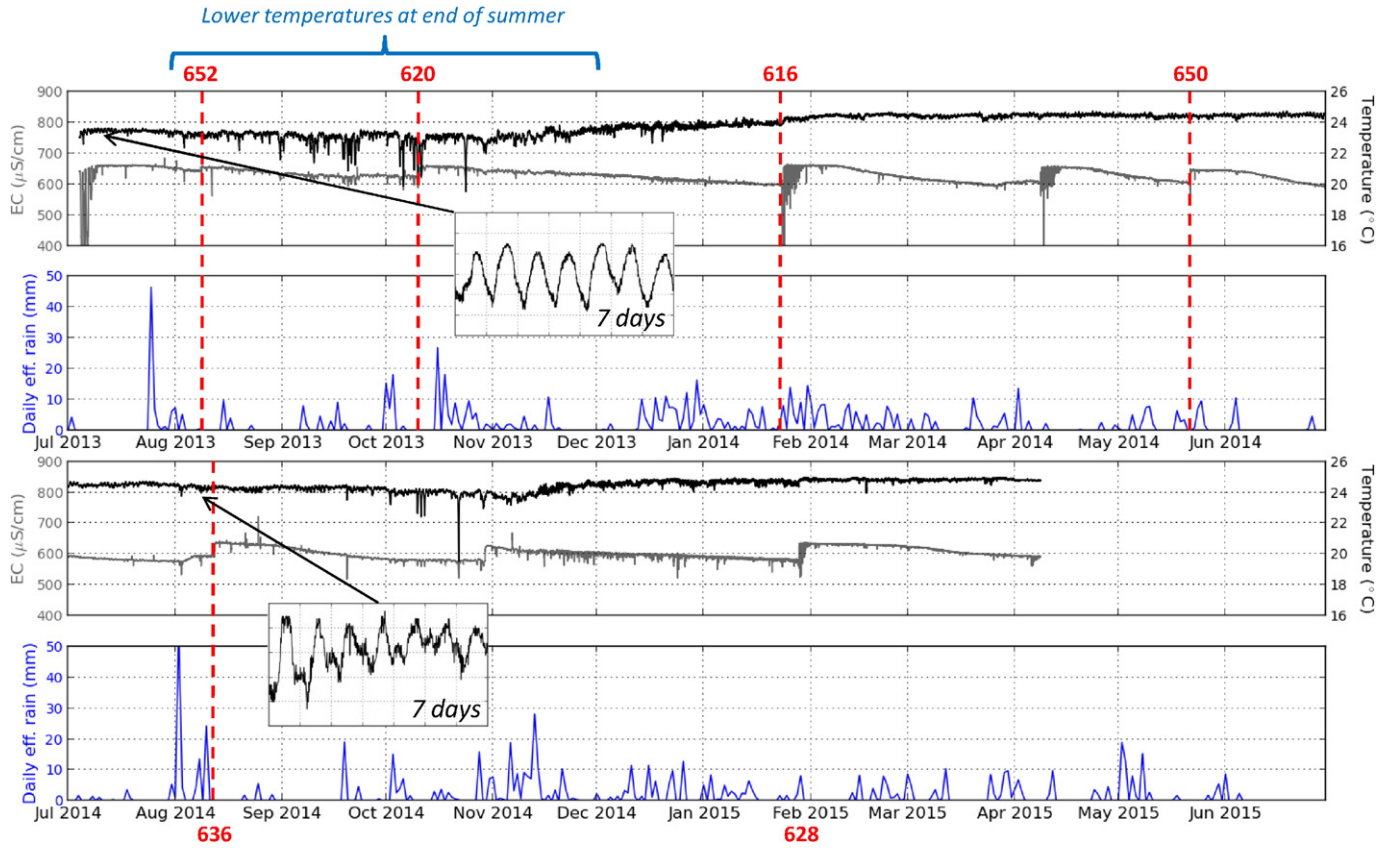

Fig. 8. Time-lapse temperature (black) and electrical conductivity (grey) for Kilbrook spring. Daily effective rainfall (blue) calculated from Met Éireann data (Dunsany synoptic station, Meath). First two panels show data from 2013 to 2014; second two panels show data from 2014 to 2015. Insets show enhanced fluctuations in temperature over two seven-day periods following the new moon on July 8th 2013 and the super full moon on August 10th 2014. Numbers in red indicate field measurements of electrical conductivity and dashed red lines indicate hydrochemical sampling rounds.

Well; this suggests that additional chloride is available to the groundwater aside from normal concentrations that may be expected from meteoric recharge and shallow groundwater (Davis et al., 1998; Freeman, 2007). This excess chloride may be from either: i) natural dissolution of evaporites, such as halite (NaCl) or sylvite (KCl); or ii) anthropogenic contamination such as the addition of fertilisers to land, de-icing of roads or industrial practises (Davis et al., 2001). Waters influenced by the dissolution of halite commonly have Cl/Br mass ratios of between 1000 and 10,000 (Davis et al., 1998). The values for Kilbrook spring are too low for this range. The excess chloride could therefore have an anthropogenic source given that waters contaminated by sewage generally have lower Cl/Br mass ratios of between 300 and 600 (Davis et al., 1998). However, no other common indicators of pollution (such as nitrates or phosphates) were routinely detected in the spring. The lack of seasonal variation in chloride argues against the application of salt to roads in winter as a source.

The origin of the salinity was further investigated by using a compositional data analysis technique to assess the relationship between Na, Cl and Br (see Blake et al., in press). This method, from Engle and Rowan (2013), uses the isometric log-ratio (ilr) transformation developed by Egozcue et al. (2003) to convert the compositional data (expressed as molar concentrations) to a new coordinate system, where each point is represented by (z_2, z_1).

$$z_1 = \frac{1}{\sqrt{2}} \ln \frac{[Na]}{[Cl]} \quad (1)$$

$$z_2 = \frac{\sqrt{2}}{\sqrt{3}} \ln \frac{\sqrt{[Na][Cl]}}{[Br]} \quad (2)$$

In the first coordinate, z_1, Br is excluded so this provides insight into the relative gain/loss of Na compared to Cl. In z_2, Br is included and this can be used to assess the degree of evaporite dissolution by the groundwater, as Br is usually excluded from the lattices of evaporite crystals, and is thus depleted in waters that gain their chloride from the dissolution of evaporites. Fig. 9 b) shows the ilr-coordinates for Na-Cl-Br for the Leinster thermal spring data from this study. These data are compared to the geochemically modelled pathway for the progressive dissolution of halite by seawater from Engle and Rowan (2013). Samples containing Na and Cl derived from the evaporation of seawater should plot down and to the left (in the negative x and y directions) of the value for modern seawater, while meteoric waters which have dissolved halite should plot up and to the right (in the positive x and y directions). The saline thermal springs (St. Edmundsbury spring and Louisa Bridge Spa Well) probably owe their excess chloride to the dissolution of evaporites (Blake et al., in press). Kilbrook spring has an intermediate chemical composition between the Ca-HCO_3-type thermal springs and the more saline springs, and contains a higher relative proportion of sodium to chloride than even the saline springs. The Kilbrook spring samples collected in the summer appear to contain more Na and less Br than samples from the winter, and could be more influenced by evaporite dissolution.

Table 1
Summary statistics for Kilbrook spring. Temperature (T) data from logger measurements. EC and pH measured in field with Hanna Combo metre during data collection rounds.

	pH range	Max EC (µS/cm)	Min EC (µS/cm)	Mean EC (µS/cm)	Max T (°C)	Min T (°C)	Mean T (°C)
Kilbrook spring	6.71–7.8	652	616	634	25.0	19.5	24.0

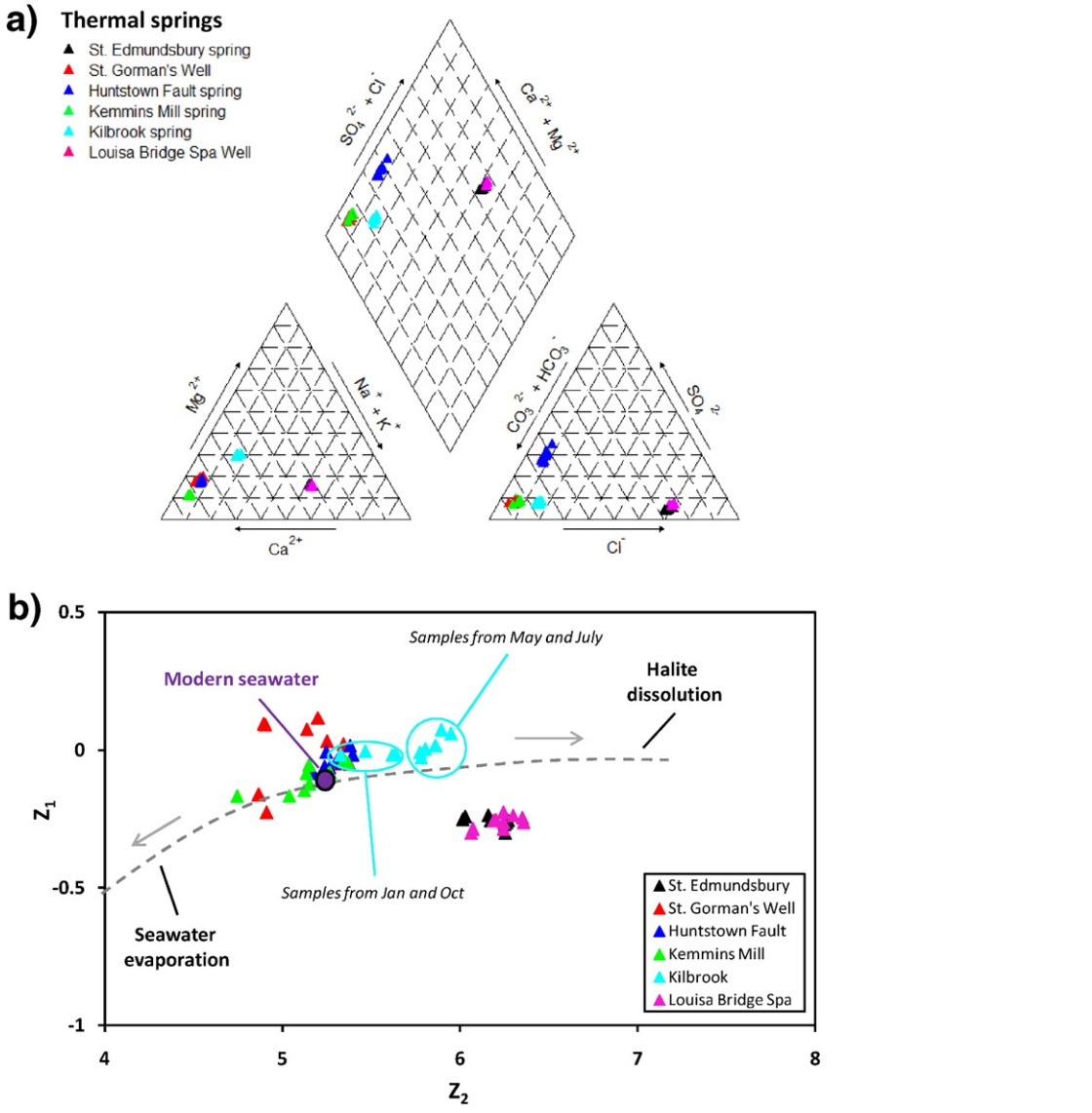

Fig. 9. a) Piper diagram of hydrochemical analyses from the Leinster thermal springs. b) Plot of ilr-coordinates (z_1, z_2) for the Na–Cl–Br system for all Leinster thermal spring data, after Blake et al. (in press); see further explanation in Section 4.2. An increase in z_2 due to a lower relative amount of Br suggests the addition of chloride through the dissolution of evaporites (halite). Geochemically modelled pathway for the progressive dissolution of halite by seawater, and modern seawater measurements after Engle and Rowan (2013).

The hydrochemical composition of Kilbrook spring probably represents the mixing of more dilute, shallower groundwaters of the Ca-HCO_3-type, and deeper, more saline, basinal fluids derived from the dissolution of chloride evaporites. Chemically, the warmer waters from the winter recharge period overlap with the other Ca-HCO_3-type thermal springs; this suggests that the winter discharges are the result of a greater degree of mixing with more dilute, shallow recharge groundwaters. The summer discharges, although slightly cooler, exhibit a greater hydrochemical influence from deep, saline groundwater.

4.3. AMT model

The published geological map of the survey area (McConnell et al., 1995) shows limestone throughout the region (Figs. 1 and 2). The resistivity values of limestone can depend upon a variety of factors, such as clay content and porosity. Unweathered limestone can generally have high resistivity values of between 1000 and 100,000 Ωm (conductivity of between 10^{-3} and 10^{-5} S/m). However, shale horizons can reduce the bulk resistivity to values as low as 10 Ωm (0.1 S/m) (Palacky, 1987). The amount of fluid contained in the rock will also reduce its bulk resistivity (Telford et al., 1990). Seawater has a low resistivity of less than 1 Ωm (>1 S/m), whereas fresh water has higher resistivities of up to 100 Ωm (0.01 S/m) (Palacky, 1987).

Even in heavily karstified regions, large cavities in limestones (caves) tend to range in size up to 10 m (Kaufmann et al., 2014), and the cavities formed in the limestones of the Dublin Basin are not expected to exceed widths of a few metres. Given the size of the cells in the AMT model mesh (50 m × 50 m in the central region of interest) the resolution is unlikely to resolve the details of the water-bearing conduits precisely. However, the presence of water-bearing conduits in a volume of limestone bedrock will reduce the bulk resistivity of the rock as a whole. In this way, the AMT method should detect structural zones and lineaments within the resistive limestone bedrock that are most likely to be water-bearing.

The main features of the geophysical model are highlighted in Fig. 10. The orientations of the structures visible in the 3-D model are broadly similar to the published geological map of the survey area, however some differences are evident. The most compelling feature in the AMT model is the NNW trending linear feature that runs through the resistive core of the model directly beneath the spring, and can be

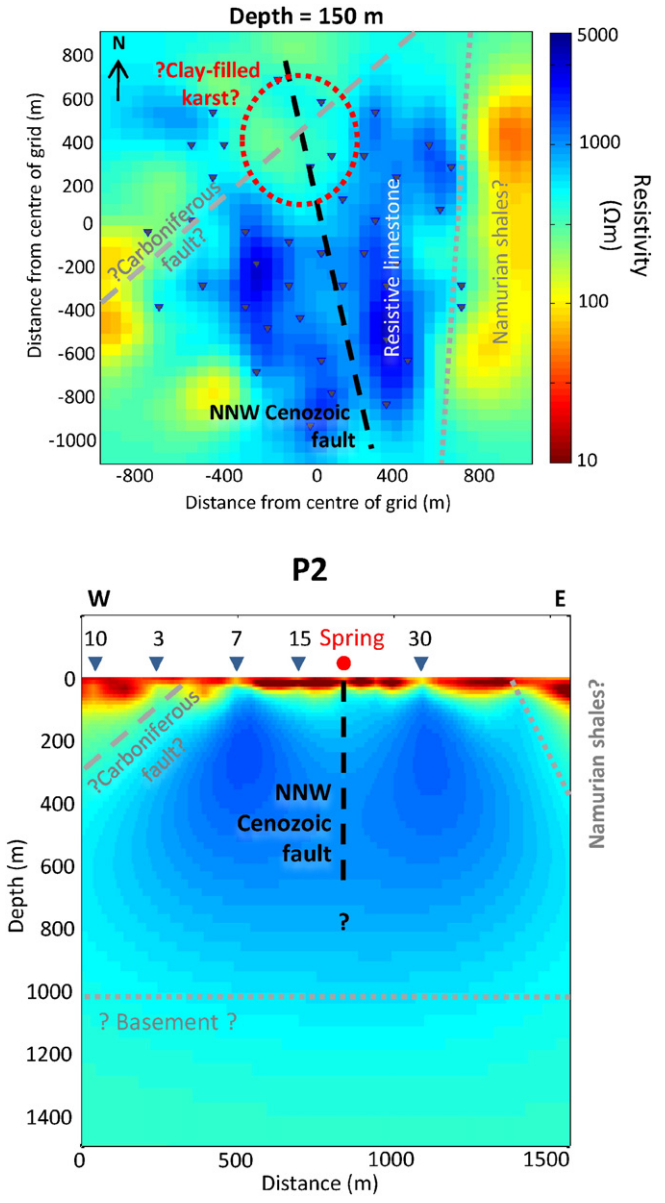

Fig. 10. Schematic diagram of the main features in the interpretation of the final 3-D AMT model.

distinguished to depths of approximately 500 m. The location and orientation of this feature corresponds closely to the inferred contact between the boundary between the Namurian shales and the Lucan Formation; however, in the geophysical model, the feature appears to have exactly the same material on either side of it. The orientation of the NNW feature is consistent with the pattern of regionally identified Cenozoic strike-slip faults. These faults are typical throughout the area of the Dublin Basin, and are known to produce very high discharges in other locations (Moore and Walsh, 2013) (e.g., Huntstown thermal spring, Fig. 1 c): see also supplementary material, Table A). The NNW feature beneath Kilbrook spring must represent the main water-bearing conduit (or a series of interconnected conduits) in the bedrock, and probably formed as a result of preferential dissolution of the limestone along a vertically pervasive Cenozoic strike-slip fault.

The resistive core in the centre of the model has resistivity values in excess of 1000 Ωm. These resistivity values are similar to values obtained for the Waulsortian Limestone Formation elsewhere in the Dublin Basin (personal observations, made at the site of St. Gorman's Well thermal spring (Fig. 1 c)). The Waulsortian Limestone Formation is resistive due to the relative purity of its carbonate and its crystalline nature. It is lithostratigraphically feasible for the Waulsortian Limestone Formation to underlie Kilbrook spring, but there is no nearby outcrop or borehole information to support this.

At shallower horizons (to depths of approx. 300 m), the NW region of the model appears to have a lower resistivity than the resistive core and could possibly represent the mapped Lucan Formation, which is expected to have a lower resistivity than the underlying Waulsortian Limestone Formation due to its higher clay content and shale-rich nature. This less resistive region appears to have a NE–SW trend, which is coincident with the mapped geological fault that runs through the survey area. This region could also owe its lower electrical resistivity to the development of water-bearing conduits in proximity to the geological fault.

A large pocket of low-resistivity material is present just north of Kilbrook spring, which extends to a depth of approx. 200 m (see Figs. 6 and 7, P1). This could represent a karstic depression in the bedrock that has been subsequently filled with unconsolidated sediments of lower resistivity that are possibly also more permeable. Large, infilled, karstic depressions have been documented in the area where Carboniferous normal faults intersect Cenozoic strike-slip faults (Moore and Walsh, 2013), albeit on a smaller scale. This depression is located where the NNW fault meets the mapped, shallow, NE–SW oriented fault, and this configuration could represent the intersection of a Cenozoic strike-slip fault and a Carboniferous normal fault, and subsequent karst development of high permeability zones along the structures (Fig. 10), as conceptualised from observations in quarries and mines in the region in Moore and Walsh (2013).

The resolution of the model lessens with increasing depth, and structure is poorly resolved below 500 m. The base of the resistive limestone appears to be located in the interval between depths of approximately 800 m and 1000 m (Fig. 10), which could tentatively represent the extent of this limestone lithology, and may even represent the extent of the Dublin Basin, and the location of the top of the more conductive basement.

4.4. Conceptual model

Information from several different strands of enquiry presented here converge on the consensus that although the thermal spring at Kilbrook does contain a deep groundwater component, the hydrothermal circulation pattern is influenced by the availability of fresh recharge waters and structurally controlled by the presence of karstified faults in the limestone bedrock.

Towards the end of the summer the temperature profile of Kilbrook spring becomes less stable with local minor drops in temperature as the regional water table rises and cooler recharge waters are made available to the hydrothermal system. With the establishment of the winter season (in November), the temperature rises slightly (to a maximum of 25.0 °C) and stabilises once more. This is probably caused by an enhanced activation of the hydrothermal circulation pattern, which occurs once the regional water table reaches some critical level. The seasonal differences in temperature support the hypothesis that the influx of cooler recharge waters to a karstic flow system in winter facilitates the operation of a relatively deep and fast circulation pattern within the bedrock, which allows cool water to infiltrate quickly to depth, become heated and mixed, and then rapidly ascend to the surface where it issues with a temperature in excess of 24 °C. In the summer the thermal waters have a lower temperature, so must not have circulated as deeply as the warmer winter waters, but their more saline hydrochemistry (Fig. 9) suggests a longer residence time and greater degree of interaction with the bedrock in a confined aquifer.

Our model has identified for the first time a significant, NNW oriented fault, of probable Cenozoic age, beneath Kilbrook spring. Given that NNW Cenozoic strike-slip faults have been identified as the main structures controlling groundwater flow in the region (Moore and Walsh,

2013), and that elsewhere in the Dublin Basin such structures have been shown to be a source of thermal groundwater (e.g., Huntstown spring in Fig. 1 c); Blake et al., in press), it is likely that the hydrothermal circulation pattern for Kilbrook spring is operating along the plane of this NNW structure (Fig. 10), although our model fails to resolve it at depths in excess of 500 m.

The intrinsically massive nature of the Waulsortian Limestone Formation allows for the development of vertical or sub-vertical dissolutional flow features, with little lateral dissipation of flow, which can facilitate the rapid transport of recharge fluids to depth, or the rapid ascent of thermal fluids to the surface. Although there is as yet no unequivocal evidence to groundtruth our AMT model, based upon the electrical resistivity values obtained for the faulted bedrock directly beneath the spring, it is possible that this could represent the Waulsortian Limestone Formation. The properties of the Waulsortian strata would allow for the formation of a deeply pervasive, vertical structure such as is imaged in our model.

The geothermal gradient of Ireland is generally poorly understood, however an average near-surface value of 25 °C/km has been suggested for the Irish Midlands by Goodman et al. (2004). In the summer, the slightly lower-temperature thermal waters (23.5 °C in 2013 and 24.5 °C in 2014) derive from a confined limestone aquifer and have a temperature that is approx. 14 °C above average. The confined source aquifer for this flow system is likely to be situated at depths in excess of 560 m, suggesting regional rather than local recharge. The high temperature fluids from the deep, confined aquifer are mixed with and diluted by cool, shallow recharge waters of meteoric origin during their ascent, so this aquifer is likely to be situated at depths much greater than 560 m.

Overall, the chemistry of the thermal spring waters indicates that the major proportion of the waters comes from a limestone source, and the hydrothermal circulation pattern must operate in limestone bedrock. Since our resistivity model appears to suggest an approximate thickness of the resistive limestone of between 800 m and 1000 m, a deep hydrothermal circulation pattern in excess of 560 m within this limestone is entirely feasible.

5. Conclusions

AMT is a proven method for investigating geothermal scenarios, and we have shown here how it may be successfully utilised as part of a cost-effective, multi-disciplinary approach to characterise a small-scale, low-enthalpy, hydrothermal system at intermediate depths (100 m to 1000 m). The interpretation of the AMT results alongside inexpensive data obtained from time-lapse temperature, chemistry and water level measurements have allowed for a better understanding of the hydrothermal circulation pattern at Kilbrook spring. Although the relatively stable and high temperatures of the spring make it an attractive candidate for geothermal energy abstraction, an important consideration for its energy potential is the large seasonal differences in discharge. Higher discharges and temperatures occur simultaneously during the winter season, when thermal energy requirements are at their maximum.

The AMT 3-D inversion results have revealed a NNW-oriented region of reduced resistivity, extending to depths of at least 500 m, which is interpreted as a water-bearing Cenozoic strike-slip fault. This structure, in combination with a shallower, NE–SW, Carboniferous normal fault in the NW region of the model, is likely to be the main facilitator of a relatively deep hydrothermal circulatory system.

Our resulting conceptual model positions the structurally controlled hydrothermal system entirely in limestone bedrock. Given the known thicknesses of the Carboniferous sediments in this area (>1000 m), this is unsurprising. In the summer, the thermal groundwater is provided by a deep, confined aquifer at depths in excess of 560 m. These thermal waters show evidence of mixing with deep, highly evolved saline waters. In the winter, the slightly higher temperatures, higher discharges, and slightly less evolved hydrochemistry (lower Na and higher Br) are provided by seasonal input of fresh recharge waters and the activation of a deep hydrothermal circulation pattern in the limestone, at depths well in excess of 560 m.

It is evident that karstification of intersecting geological structures within the limestone bedrock has been the main factor in the development of a thermal spring at Kilbrook. If the Irish thermal springs are to be exploited in the future for geothermal energy purposes, it is vital to gain a thorough understanding of the local and regional structural geology at shallow and deep levels, in order to effectively target this geothermal energy resource. This paper has demonstrated how an electromagnetic geophysical technique such as AMT can greatly help in this regard. Since the Irish thermal springs occur in limestone bedrock, their hydrothermal circulation patterns are likely to be centred on the intersection of geological structures, and therefore a 3-D deployment of AMT stations followed by 3-D inversion could be an optimal strategy for similar surveys in the future.

Acknowledgements

This work was carried out as part of the IRETHERM project, which is funded by Science Foundation Ireland (grant number 10/IN.1/I3022), in collaboration with the IRETHERM team (www.iretherm.ie). We would like to thank the interns, staff and students at DIAS who helped with data acquisition, and various landowners for granting us access to their land.

Appendix A. Supplementary data

Supplementary data to this article can be found online at http://dx.doi.org/10.1016/j.jappgeo.2016.06.007.

References

Aldwell, C.R., Burdon, D.J., 1980. Hydrogeothermal Conditions in Ireland. XXVI International Geological Congress, Paris; Fossil Fuels Sec. 14.2; 14.0068:21.

Arango, C., Marcuello, A., Ledo, J., Queralt, P., 2009. 3D magnetotelluric characterization of the geothermal anomaly in the Llucmajor aquifer system (Majorca, Spain). J. Appl. Geophys. 68, 479–488.

Barcelona, H., Favetto, A., Peri, V.G., Pomposiello, C., Ungarelli, C., 2013. The potential of audiomagnetotellurics in the study of geothermal fields: a case study from the northern segment of the La Candelaria range, northwestern Argentina. J. Appl. Geophys. 88, 83–93.

Barham, M., Murray, J., Sevastopulo, G.D., Williams, D.M., 2015. Conodonts of the genus Lochriea in Ireland and the recognition of the Viséan–Serpukhovian (carboniferous) boundary. Lethaia 48 (2), 151–171.

Blake, S., Henry, T., Murray, J., Flood, R., Muller, M., Jones, A.G., Rath, V., 2016. Investigating the provenance of thermal groundwater using compositional multivariate statistical analysis: a hydrogeochemical study from Ireland. Appl. Geochem. http://dx.doi.org/10.1016/j.apgeochem.2016.05.008.

Bodvarsson, G., 1970. Confined fluids as strain meters. J. Geophys. Res. 75 (14), 2711–2718.

Burdon, D.J., 1983. Irish Geothermal Project, Phase 1. Geological Survey of Ireland, Dublin. Report 150/75/15.

Caldwell, G.T., Bibby, H.M., Brown, C., 2004. The magnetotelluric phase tensor. Geophys. J. Int. 158, 457–469.

Campanyà, J., Ogaya, X., Jones, A.G., Rath, V., Vozar, J., 2016. The advantages of complementing MT profiles in 3-D environments with geomagnetic transfer function and inter-station horizontal magnetic transfer function data: results from a synthetic case study. Geophys. J. Int. (in review).

Chave, A.D., Jones, A.G., 2012. Introduction to the Magnetotelluric Method. In: Chave, A.D., Jones, A.G. (Eds.), The Magnetotelluric Method. Cambridge University Press, U.K., pp. 1–18.

Chew, D.M., Strachan, R.A., 2014. The Laurentian Caledonides of Scotland and Ireland. In: Corfu, F., Gasser, D., Chew, D.M. (Eds.), New Perspectives on the Caledonides of Scandinavia and Related Areas. Geological Society of London Special Publications 309, pp. 45–91.

Davis, S.N., Whittemore, D.O., Fabryka-Martin, J., 1998. Uses of chloride/bromide ratios in studies of potable water. Ground Water 36, 338–350.

Davis, S.N., Cecil, L.D., Zreda, M., Moysey, S., 2001. Chlorine-36, bromide, and the origin of spring water. Chem. Geol. 179, 3–16.

de Morton, S.N., Wallace, M.W., Reed, C.P., Hewson, C., Redmond, P., Cross, E., Moynihan, C., 2015. The significance of Tournaisian tectonism in the Dublin basin: implications for basin evolution and zinc-lead mineralization in the Irish midlands. Sediment. Geol. 330, 32–46.

Egbert, G.D., Kelbert, A., 2012. Computational recipes for electromagnetic inverse problems. Geophys. J. Int. 189, 251–267.
Egozcue, J.J., Pawlowsky-Glahn, V., Mateu-Figueras, G., Barceló-Vidal, C., 2003. Isometric logratio transformations for compositional data analysis. Math. Geol. 35, 279–300.
Engle, M.A., Rowan, E.L., 2013. Interpretation of Na–Cl–Br systematics in sedimentary basin brines: comparison of concentration, element ratio, and isometric log-ratio approaches. Math. Geosci. 45, 87–101.
Falgàs, E., Ledo, J., Benjumea, B., Queralt, P., Marcuello, A., Teixidó, T., Martí, A., 2011. Integrating hydrogeological and geophysical methods for the characterization of a deltaic aquifer system. Surv. Geophys. 32, 857–873.
Farquharson, C.G., Craven, J.A., 2009. Three-dimensional inversion of magnetotelluric data for mineral exploration: an example from the McArthur River uranium deposit, Saskatchewan, Canada. J. Appl. Geophys. 68, 450–458.
Freeman, J.T., 2007. The use of bromide and chloride mass ratios to differentiate salt-dissolution and formation brines in shallow groundwaters of the Western Canadian Sedimentary Basin. Hydrogeol. J. 15, 1377–1385.
Gamble, T.D., Goubau, W.M., Clarke, J., 1979. Magnetotellurics with a remote reference. Geophysics 44 (1), 53–68.
García, X., Jones, A.G., 2005. A new methodology for the acquisition and processing of audio-magnetotelluric (AMT) data in the AMT dead band. Geophysics 70 (5), G119–G126.
Goodman, R., Jones, G., Kelly, J., Slowey, E., O'Neill, N., 2004. Geothermal Energy Resource Map of Ireland Final Report. Sustainable Energy Ireland (SEI), Dublin.
Graham, J.R., 2009. Devonian. In: Holland, C.H., Sanders, I.S. (Eds.), The Geology of Ireland, second ed. Dunedin Academic Press Ltd., Edinburgh, pp. 175–214.
Henry, T., 2014. An Integrated Approach to Characterising the Hydrogeology of the Tynagh Mine Catchment, County Galway, Ireland. (Ph.D. thesis), National University of Ireland Galway (unpublished).
Hitzman, M.W., 1999. Extensional Faults that Localized Syndiagenetic Zn–Pb Deposits and their Reactivation during Variscan Compression. In: McCaffrey, K.J., Lonergan, L., Wilkinson, J.J. (Eds.), Fractures, Fluid Flow and Mineralization. Geological Society of London Special Publication 155, pp. 233–245.
Hunter Williams, N., Misstear, B., Daly, D., Johnston, P., Lee, M., Cooney, P., Hickey, C., 2011. A National Groundwater Recharge Map for Ireland. Proceedings National Hydrology Conference. Irish National Committees for the IHP and ICID, pp. 89–109.
Jones, A.G., 1986. Parkinson's pointers' potential perfidy! Geophys. J. R. Astron. Soc. 87, 1215–1224.
Jones, A.G., 2011. Three-dimensional galvanic distortion of three-dimensional regional conductivity structures: comment on "three-dimensional joint inversion for magnetotelluric resistivity and static shift distributions in complex media" by Yutaka Sasaki and max a Meju. J. Geophys. Res. Solid Earth 116.
Jones, A.G., Jödicke, H., 1984. Magnetotelluric Transfer Function Estimation Improvement by a Coherence-Based Rejection Technique. 54th Annual International SEG Meeting. Society of Exploration Geophysicists, Atlanta, Georgia Abstract Volume, pp. 51–55.
Jones, A.G., Chave, A.D., Egbert, G., Auld, D., Bahr, K., 1989. A comparison of techniques for magnetotelluric response function estimation. J. Geophys. Res. Solid Earth Planets 94, 14201–14213.
Kalscheuer, T., Blake, S., Podgorski, J.E., Wagner, F., Green, A.G., Maurer, H., Jones, A.G., Muller, M., Ntibinyane, O., Tshoso, G., 2015. Joint inversions of three types of electromagnetic data explicitly constrained by seismic observations: results from the central Okavango Delta, Botswana. Geophys. J. Int. 202, 1429–1452.
Kaufmann, G., Gabrovšek, F., Romanov, D., 2014. Deep conduit flow in karst aquifers revisited. Water Resour. Res. 50, 4821–4836.
Kelbert, A., Meqbel, N., Egbert, G.D., Tandon, K., 2014. ModEM: a modular system for inversion of electromagnetic geophysical data. Comput. Geosci. 66, 40–53.
Kiyan, D., Jones, A.G., Vozar, J., 2014. The inability of magnetotelluric off-diagonal elements to sense oblique conductors in 3-D. Geophys. J. Int. 196, 1351–1364.
Lai, G., Ge, H., Wang, W., 2013. Transfer functions of the well-aquifer systems response to atmospheric loading and earth tide from low to high-frequency band. J. Geophys. Res. Solid Earth 118, 1904–1924.
Lees, A., Miller, J., 1995. Waulsortian Banks. In: Monty, C.L.V., Bosence, D.W.J., Bridges, P.H., Pratt, B.R. (Eds.), Carbonate Mud-Mounds: their Origin and EvolutionSpecial Publication of the International Association of Sedimentologists 23. Blackwell Science, Oxford, pp. 191–271.
Maréchal, J., Sarma, M., Ahmed, S., Lachassagne, P., 2002. Establishment of earth tides effect on water level fluctuations in an unconfined hard rock aquifer using spectral analysis. Curr. Sci. 83 (1), 101–104.
Marchant, T.R., Sevastopulo, G.D., 1980. The Calp of the Dublin district. J. Earth Sci. Roy. Dublin Soc. 5, 195–203.
MacDermot, C.V., Sevastopulo, G.D., 1972. Upper Devonian and lower carboniferous stratigraphical setting of Irish mineralization. Geol. Surv. Ireland Bull. 1, 267–280.
McConnell, B., Philcox, M.E., MacDermott, C.V., Sleeman, A.G., 1995. Bedrock Geology 1: 100,000 Scale Map, Sheet 16, Kildare - Wicklow. Geological Survey of Ireland, Dublin.
Meqbel, N.M., Egbert, G.D., Wannamaker, P.E., Kelbert, A., 2014. Deep electrical resistivity structure of the northwestern U.S. derived from 3-D inversion of USArray magnetotelluric data. Earth Planet. Sci. Lett. 402, 290–304.
Mooney, B., Allen, A., Koniger, P., 2010. Investigation of Source and Conduit for Warm Geothermal Waters, North Cork, Republic of Ireland. Proceedings World Geothermal Conference, Bali, Indonesia.
Moore, J.P., Walsh, J.J., 2013. Analysis of fracture systems and their impact on flow pathways in Irish bedrock aquifers. Geol. Surv. Ireland Groundw. Newsl. 51, 28–33.
Moore, J.P., Walsh, J.J., Manzocchi, T., Hunter Williams, T., Ofterdinger, U., Ball, D., 2015. Quantitative Analysis of Faults and Fracture Systems and their Impact on Groundwater Flow in Irish Bedrock Aquifers. Proceedings of EGU 2015 17, EGU2015–13965-2.
Murphy, F.X., Brück, P., 1989. An Investigation of Irish Low Enthalpy Geothermal Resources with the Aid of Exploratory Boreholes. Report 98/13.
Palacky, G.J., 1987. Resistivity Characteristics of Geologic Targets. In: Nabighian, M.N. (Ed.), Electromagnetic Methods in Applied Geophysics Theory: Tulsa, Okla. Society of Exploration Geophysicists 1, pp. 53–129.
Piña-Varas, P., Ledo, J., Queralt, P., Marcuello, A., Bellmunt, F., Hidalgo, R., Messeiller, M., 2014. 3-D magnetotelluric exploration of Tenerife geothermal system (Canary Islands, Spain). Surv. Geophys. 35 (4), 1045–1064.
Rojstaczer, S., Agnew, D.C., 1989. The influence of formation material properties on the response of water levels in wells to earth tides and atmospheric loading. J. Geophys. Res. 94 (B9), 12403–12411.
Schmucker, U., 1970. Anomalies of Geomagnetic Variations in the Southwestern United States. Journal of Geomagnetic Oceanography. University of California Press, Berkeley, USA.
Sevastopulo, G.D., 2009. Carboniferous: Mississippian (Serpukhovian) and Pennsylvanian. In: Holland, C.H., Sanders, I.S. (Eds.), The Geology of Ireland, second ed. Dunedin Academic Press, Edinburgh, pp. 269–294.
Sasaki, Y., Meju, M.A., 2006. Three-dimensional joint inversion for magnetotelluric resistivity and static shift distributions in complex media. J. Geophys. Res. Solid Earth 111 (11 pp.).
Sevastopulo, G.D., Wyse Jackson, P.N., 2009. Carboniferous (Dinantian). In: Holland, C.H., Sanders, I.S. (Eds.), The Geology of Ireland, second ed. Dunedin Academic Press Ltd., Edinburgh, pp. 241–288.
Simpson, F., Bahr, K., 2005. Practical Magnetotellurics. Cambridge University Press, United Kingdom.
Siripunvaraporn, W., Egbert, G., 2009. WSINV3DMT: vertical magnetic field transfer function inversion and parallel implementation. Phys. Earth Planet. Inter. 173, 317–329.
Somerville, I.D., 2008. Biostratigraphic zonation and correlation of Mississippian rocks in Western Europe: some case studies in the late Viséan/Serpukhovian. Geol. J. 43, 209–240.
Somerville, I.D., Strogen, P., Jones, G.L., 1992. Mid-Dinantian Waulsortian buildups in the Dublin Basin, Ireland. Sediment. Geol. 79, 91–116.
Strogen, P., Somerville, I.D., Pickard, N.A.H., Jones, G.L.L., Fleming, M., 1996. Controls on Ramp, Platform and Basinal Sedimentation in the Dinantian of the Dublin Basin and Shannon Trough, Ireland. In: Strogen, P., Somerville, I.D., Jones, G.L.L. (Eds.), Recent Advances in Lower Carboniferous Geology. Geological Society, London, Special Publication 107, pp. 263–279.
Telford, W.M., Geldart, L.P., Sheriff, R.E., 1990. Applied Geophysics. second ed. Cambridge University Press, Cambridge U.K.
Walsh, S., 2012. A Summary of Climate Averages 1981–2010 for Ireland. Climatological Note No.14. Met Éireann, Dublin.
Wilkinson, J.J., 2010. A review of fluid inclusion constraints on mineralization in the Irish ore field and implications for the genesis of sediment-hosted Zn-Pb deposits. Econ. Geol. 105, 417–442.
Worthington, R.P., Walsh, J.J., 2011. Structure of lower carboniferous basins of NW Ireland, and its implications for structural inheritance and Cenozoic faulting. J. Struct. Geol. 33, 1285–1299.
Zhang, L., Hao, T., Xiao, Q., Wang, J., Zhou, L., Qi, M., Cui, X., Cai, N., 2015. Magnetotelluric investigation of the geothermal anomaly in Hailin, Mudanjiang, northeastern China. J. Appl. Geophys. 118, 47–65.